


RESEARCH

Open Access



T-lymphocytes suppression by CD14⁺ monocytes with high expression of ULK2 in patients with multiple myeloma

Fengping Peng^{1,2,3}, Zhaoyun Liu^{1,2,3*}, Fengjuan Jiang^{1,2,3}, Nianbin Li^{1,2,3}, Hao Wang^{1,2,3}, Nanhao Meng^{1,2,3}, Hui Liu^{1,2,3}, Kai Ding^{1,2,3} and Rong Fu^{1,2,3*} 

Abstract

Background Multiple myeloma (MM), a plasma cell malignancy, remains incurable and is highly prone to relapse. Immunosuppressive cells in the bone marrow environment inhibit endogenous T-lymphocytes activity and reduce the efficacy immunotherapies. Abnormal bone marrow monocytes in MM have been associated with inferior outcomes. This study explored the mechanism of T-lymphocytes suppression by bone marrow CD14⁺ monocytes in MM.

Methods Single-cell RNA sequence data (GSE124310) derived from MM samples were analyzed. CD14⁺ monocytes from the bone marrow of patients with newly-diagnosed MM were detected, and RNA sequencing was performed. Interactions between CD14⁺ monocytes and T-lymphocytes, as along with the corresponding downstream signaling mechanism, were assessed through in vitro and in vivo experiments.

Results The alterations in MHC II signaling related to outgoing interaction were decreased in CD14⁺ monocytes from patients with MM. Abnormal numbers, defective antigen presentation, and downregulated surface co-stimulatory molecules in bone marrow CD14⁺ monocytes were also observed. RNA sequencing identified upregulated expression of Unc-51 like autophagy activating kinase 2 (*ULK2*) in these monocytes, a protein involved in the antigen processing and presentation pathway. CD14⁺ monocytes from patients with NDMM suppressed T-lymphocyte activity, and treatment of CD14⁺ monocytes with a ULK1/ULK2 inhibitor alleviated this suppression. MM xenograft model showed that CD14⁺ monocytes high-expressing *ULK2* suppressed T-lymphocytes and promoted tumor growth.

Conclusion We demonstrated that CD14⁺ monocytes from MM can disrupt the delivery of antigenic peptides through the antigen processing and presentation pathway. This disruption affects T-lymphocytes activity and attenuates their ability to kill malignant cells and secrete cytokines. These findings lay the foundation for understanding the immuno-suppressive environment in MM, improving the efficacy of immunotherapy based on T-lymphocytes, and developing new therapeutic targets.

Keywords Multiple myeloma, CD14⁺ monocytes, T-lymphocytes, ULK2

*Correspondence:

Zhaoyun Liu
liuzhaoyun114@163.com
Rong Fu
furong8369@tmu.edu.cn

Full list of author information is available at the end of the article



© The Author(s) 2025. **Open Access** This article is licensed under a Creative Commons Attribution-NonCommercial-NoDerivatives 4.0 International License, which permits any non-commercial use, sharing, distribution and reproduction in any medium or format, as long as you give appropriate credit to the original author(s) and the source, provide a link to the Creative Commons licence, and indicate if you modified the licensed material. You do not have permission under this licence to share adapted material derived from this article or parts of it. The images or other third party material in this article are included in the article's Creative Commons licence, unless indicated otherwise in a credit line to the material. If material is not included in the article's Creative Commons licence and your intended use is not permitted by statutory regulation or exceeds the permitted use, you will need to obtain permission directly from the copyright holder. To view a copy of this licence, visit <http://creativecommons.org/licenses/by-nc-nd/4.0/>.

Introduction

Multiple myeloma (MM) is the second most common hematological neoplasm. MM is incurable, and almost all patients experience relapse or become refractory [1]. The compromised bone marrow environment in MM is closely related to reduced response to therapy, chemotherapy resistance, and disease progression [2]. Insufficient antibody production, uncontrollable T and NK lymphocyte compartments, dysfunctional antigen processing and presentation, upregulated inhibitory ligands (such as PD-L1), and recruited immunosuppressive cells (such as regulatory T cells and myeloid-derived suppressor cells) are some of the features of immune escape in MM [3]. Maura et al. [4] found that the baseline proportion of NK cells, a higher baseline diversity of T-cell receptors, the disappearance of sustained immune activation, and durable monocyte expansion predicted the prognosis and remission depth in patients with newly-diagnosed MM (NDMM) treated with anti-CD38 antibodies-based immunotherapy regimens. Botta et al. [5] indicated that multiple immune checkpoint factors such as PD-1, LAG3, and TIGIT were expressed in large T-cell clones from MM, serving as predictors for the response to lenalidomide-based treatment. Friedrich et al. [6] revealed that the response of patients with MM receiving B-cell maturation antigen (BCMA) bispecific antibodies was associated with loss of target cell antigens and of MHC class I, as well as an increase in exhausted CD8⁺ T lymphocyte clones in the bone marrow environment. Dhodapkar et al. [7] reported that the lower diversity of the T-cell receptor repertoire, exhaustion of endogenous marrow T-lymphocytes, and the presence of immune-suppressive myeloid cells affected the long-term response following Chimeric Antigen Receptor T-cell Immunotherapy (CART) in MM. The deficiency, dysfunction, exhaustion, and senescence of T-lymphocytes that occur in MM are key factors in the disruption of the immune system [8], and this partially limits the potential application and efficacy of novel immunotherapeutic modalities. In summary, improving T-lymphocyte status in MM is essential for enhancing the depth and duration of the therapeutic response.

Numerous studies have indicated that myeloid cells promote, support, and maintain cancer cell growth by interacting with tumor cells, altering T-lymphocyte composition and activity, and manipulating stromal architecture [9]. Moreover, monocytes serve as the primary source of macrophages and dendritic cells, contributing to immune escape by differentiating into immune regulatory cells within the tumor environment [10]. Bone marrow CD14⁺ monocytes in patients with MM are associated with a short progression-free and overall survival [11]. Malignant plasma cells from patients with relapsed/

refractory MM generate a suppressive immune microenvironment by upregulating inflammatory cytokines and interacting closely with myeloid cells, particularly CD14⁺ and CD16⁺ monocytes [12]. Li et al. [13] indicated that the CD14⁺ monocyte-macrophages subpopulation increased in patients with relapsed MM following BCMA CART treatment, as revealed by single-cell sequencing. This cell subpopulation exhibits a pro-tumorigenic phenotype, induces T-lymphocyte exhaustion, and plays a crucial role in relapse after CART treatment.

Monocytes play a crucial role in innate and adaptive immune responses, including immune cell activation, phagocytosis, antigen presentation, production of pro-inflammatory cytokines, and patrolling [14]. Consequently, we investigated the role of bone marrow monocytes in MM as a key factor in the suppression of T-lymphocytes to address current clinical challenges. We observed abnormalities in the proportion and functions of bone marrow CD14⁺ monocytes in patients with NDMM. RNA sequencing revealed upregulation of Unc-51 like autophagy activating kinase 2 (*ULK2*) expression in these CD14⁺ monocytes. ULK2 is a serine/threonine protein kinase, which mediates autophagy under starvation conditions [15]. The high expression of *ULK2* in CD14⁺ monocytes from MM was involved in defective antigen presentation and downregulation of co-stimulatory molecules, which affected the activity of T-lymphocytes.

Methods and materials

Analysis of single-cell RNA sequence data

Bone marrow samples of datasets from patients with NDMM (n = 7) and healthy donors (normal bone marrow [NBM], n = 9) were obtained from Gene Expression Omnibus (GSE124310). Cell clusters, cell communication, gene ontology (GO) enrichment, and differential gene expression analyses were performed using the R package Seurat (Version 4.3.0), ClusterProfiler (Version 4.10.1), and CellChat (Version 2.1.2). Preprocessing of single-cell RNA sequence data was performed as previously described [2]. For the analysis of cell interactions, expression levels were assessed relative to the total reads mapped to the same group of coding genes across the entire transcriptome. The expression levels within each single-cell cluster were averaged.

Study population and data collection

The study was approved by the Ethics Committee of the General Hospital of Tianjin Medical University (Approval No. IRB2023-KY-325). Bone marrow samples were obtained from patients with NDMM (n = 45) and healthy controls (HCs, n = 20) who had been hospitalized in the Hematology Department of Tianjin Medical University

General Hospital between May 2023 and February 2024. Written informed consent was obtained from all patients, in accordance with the tenets of the Declaration of Helsinki. Patient characteristics are shown in Table 1.

Detection of bone marrow CD14⁺ monocytes by flow cytometry

Bone marrow samples from patients with NDMM and HCs were collected. Erythrocytes were lysed, and dead cells were identified using a Zombie NIR™ Fixable Viability Kit (Cat# 423105, BioLegend, USA). Monocytes were detected via flow cytometry using Beckman CytoFLEX equipment and analyzed using FlowJo software. The antibodies used for cell marker staining were the following: anti-human CD14 PE (Cat# 325606), anti-human CD16 APC (Cat# 360706), anti-human CD38 FITC (Cat# 356610), anti-human CCR2 BV421 (Cat# 357210), anti-human CD86 BV510 (Cat# 305432), anti-human CD80 PE-Cy7 (Cat# 375408), anti-human HLA-DR PerCP (Cat# 307628), all of them from BioLegend, USA.

Magnetic bead sorting of bone marrow CD14⁺ monocytes
Bone marrow samples (10 mL) from patients with NDMM and HCs were collected and processed. Mononuclear cells were isolated using density gradient

centrifugation with a lymphocyte isolation solution and counted after erythrocyte lysing. The cells were incubated with an appropriate volume of CD14 magnetic beads (Miltenyi, 130-050-201, Germany) and sorted using a magnetic separation technique. Purity of the monocyte preparation was analyzed through flow cytometry with antibodies against human CD14 PE and human CD138 BV421 (Cat# 356516, BioLegend).

High-throughput RNA sequencing

Primary CD14⁺ monocytes were collected, sorted, and preserved in Trizol (Invitrogen, USA) at − 80° C. RNA sequencing was performed at Novogene Co., Ltd., China, and the results were analyzed for gene enrichment. The datasets were stored in the SRA public repository: <https://www.ncbi.nlm.nih.gov/sra/PRJNA1138781>.

Western blot

Proteins were extracted using RIPA lysis buffer (Solarbio, China) and their concentration was quantified using a BCA protein assay kit (CoWin Biosciences, China). They were then separated by SDS-PAGE and transferred to a 0.45 μM PVDF membrane (Millipore, USA). The membranes were blocked with 5% skimmed milk in TBST (0.1% Tween 20) for 1 h., followed by overnight incubated

Table 1 Clinical data of patients with Newly-diagnosed multiple myeloma

Characteristics	Patients
Number	45
Gender	
Male	19 (42%)
Female	26 (58%)
Age (year)	68 (36–82)
Types of MM	IgG (26), IgA (4), IgD (1), light-chain (14)
Stage of pre-treatment	
Durie-Salmon (DS)	IA 1 (2%), IIA 7 (16%), IIIA 23 (51%), IIIB 14 (31%)
International Staging System (ISS)	
	I5 (11%), II 11(24%), III 29 (65%)
Revised ISS (R-ISS)	
	I3 (7%), II 18 (40%), III 24 (53%)
Parameters of pre-treatment	
Creatinine clearance > 30 ml/min	29 (64%)
Creatinine clearance ≤ 30 ml/min	16 (36%)
Hemoglobin ≥ 100 g/l	11 (24%)
Hemoglobin < 100 g/l	34 (76%)
Calcium > 2.75 mmol/l	11 (24%)
Calcium ≤ 2.75 mmol/l	34 (76%)
Peripheral blood absolute monocyte count (*10 ⁹ /L)	
0.1- < 0.6	30 (67%)
0.6- < 1.0	10 (22%)
≥ 1.0	5 (11%)

at 4 °C with primary antibodies. After washing three times with TBST, enzyme-labelled secondary antibodies were added and the membranes were incubated at room temperature for 1 h. Finally, the membranes were washed three times with TBST, and the protein bands were visualized using a gel imaging system. The following antibodies were used in the procedure: anti-DYKDDDDK Tag (Sigma, Cat# F1804, 1:1000), anti- β -actin (CST, Cat# 8457 1:1000), anti-vinculin (CST, Cat# 13901, 1:1000), ULK2 (ABclonal, Cat# A15243, 1:1000), anti-MHC I (Abways, Cat# 6702, 1:1000), anti-MHC II (Abways, Cat# 6763, 1:2000), anti-TAP1 (CST, Cat# 49761 T, 1:1000), anti-PSME1 (Abways, Cat# CY8056, 1:1000), anti-CTSB (Abways, Cat# CY6772, 1:1000), anti-CTSL (Abways, Cat# CY6745, 1:1000), HRP-conjugated goat anti-rabbit IgG (CST, Cat# 7074, 1:3000) and goat anti-mouse IgG (CST, Cat# 7074, 1:3000).

Real-time quantitative PCR

Total RNA was extracted using Trizol, and cDNA was synthesized by Hifair III 1st Strand cDNA Synthesis SuperMix (Cat# 11141ES60, Yeasen, China). Real-time quantitative (RT-qPCR) was performed using a Bio-Rad iQ5 Real-time system with Hieff UNICON Universal Blue qPCR SYBR Green Master Mix (Cat# 11184ES08, Yeasen, China). Each sample was run in triplicate. GAPDH mRNA served as a housekeeping gene. The primers were synthesized by Sangon Biotech (Shanghai, China), and their sequences are shown in Table S1.

Lentiviral infection

The human acute monocytic leukemia THP1 cell line (ATCC, TIB-202) was cultured with RPMI-1640 medium (Gibco, USA) supplemented with 10% fetal bovine serum (FBS, OriCell, China), 0.05 mM 2-mercaptoethanol, and 1% Penicillin–Streptomycin, in a 5% CO₂ incubator at 37 °C. HBLV-h-ULK2-3 \times flag-mcherry-Puro and HBLV-mCherry-Puro-empty vectors lentivirus were purchased from Shanghai Hanheng Biotechnology. THP1 cells were infected with the lentiviral vectors along with 1 μ g/mL polybrene in 24-well plates, centrifuged at 1000 g, for 1 h at 32 °C, and added with 1 μ g/mL puromycin after 72 h to select the stably transfected cells. Flow cytometry, PCR and western blot (WB) were used to confirm *ULK2* expression in the transfected cells. THP1 cells over-expressing *ULK2* (oeULK2) were cultured for 48 h in a medium containing a concentration of 0.5 μ M, 0.25 μ M, or 0.125 μ M of the ULK1/ULK2 inhibitor MRT68921 (HY-100006 A, MCE, USA).

Co-culture of CD14⁺ monocytes and CD3⁺ T-lymphocytes

Bone marrow mononuclear cells from 12 patients with NDMM were collected and sorted to isolate CD14⁺

monocytes and CD3⁺ T-lymphocytes. Mononuclear cells were isolated and incubated with an appropriate volume of either CD14 or CD3 magnetic beads (Pan-T cell isolation Kit, Miltenyi, 130-096-535, Germany). Subsequently, the cells were sorted using a magnetic separation technique. The purity of the lymphocyte preparation was analyzed through flow cytometry using antibodies against human CD3 FITC (Cat# 317306, BioLegend). CD3⁺ T-lymphocytes were activated with humanized 4 μ g/mL anti-human CD3 and anti-human CD28 (Cat# TL-101 and TL-102, T&L Biological Technology) monoclonal antibodies, and cultured in RPMI-1640 medium, with 10% heat-inactivated FBS, 1% penicillin/streptomycin, 1 mM sodium pyruvate, 1% minimum essential medium with nonessential amino acids, 0.05 mM 2-mercaptoethanol, 2 mM L-glutamine, and 25 mM HEPES, supplemented with 20 IU/ml IL2 (Cat# 200-02-100 μ g, PeproTech, USA). The primary CD14⁺ monocytes were pretreated with 0.25 μ M MRT68921 in complete RPMI-1640 medium for 48 h, then co-cultured with lymphocytes in a 1:1 ratio for 48 h. T lymphocytes were detected by flow cytometry and analyzed using FlowJo software. The antibodies used for cell marker staining were the following: anti-human CD8 FITC (Cat# 344704), anti-human CD4 PerCP (Cat# 317432), anti-human CD14 PE, anti-human Granzyme B BV421 (Cat# 396414), anti-human CD69 BV510 (Cat# 310936), anti-human TNF α PE-Cy7 (Cat# 502930), anti-human CD25 APC (Cat# 385605), all of them from BioLegend.

Mouse model

Twenty NOG (NOD-Cg-*Prkdc*^{scid}*IL2rg*^{tm1 sug}/JicCr1, 5–7 weeks old) mice were purchased from Beijing Vital River Laboratory Animal Technology Co., Ltd., China (Experimental Animal Welfare Ethics Committee Approval No. IRB2023-DWFL-397). The experimental mice were subcutaneously implanted with 5 \times 10⁶ RPMI-8226 MM cells and randomly allocated to five different groups with a similar starting tumor volume of approximately 40 mm³ (n = 4 per group, Fig. 5A). MM bone marrow activated CD3⁺ T cells (1 \times 10⁷) and *ULK2*^{high} or *ULK2*^{low/-} CD14⁺ monocytes were mixed at a ratio of 1:3 and injected via the tail vein. Tumor size was measured using a caliper every three days, and the study was terminated after two weeks. The mice were euthanized, serum samples were collected for the evaluation of interferon (IFN γ) levels, and infiltrating lymphocytes of tumor tissues were stained with Zombie-NIR, TruStain FcXTM (anti-human CD16/32) antibody (Cat# 163404), anti-human CD45 PerCP (Cat# 304026), anti-human CD3 FITC, anti-human CD69 BV510, anti-human GZMB BV421, and anti-human TNF α PE Cy7 antibodies (BioLegend), and detected using flow cytometry.

Statistical analysis

Statistical analyses were performed using GraphPad Prism 8. An unpaired Student's t-test, a one-way ANOVA test, or a two-way ANOVA test were used to compare differences between groups. The correlation of the data was described using Pearson's correlation coefficient (r). A p -value less than 0.05 was considered statistically significant.

Results

Abnormal numbers and functional defects of bone marrow CD14⁺ monocytes from patients with NDMM

By analyzing the data of GSE124310, 11 cell clusters were defined by marker gene expression patterns (Fig. 1A, Supplementary Figure S1). We found that the incoming and outgoing signal strength of bone marrow CD14⁺ monocytes from patients with MM were increased compared to those from healthy donors (NBM, Fig. 1B). The change in MHC II gene signaling of outgoing interaction in CD14⁺ monocytes was decreased in MM (Fig. 1C). The top ten GO enrichments for differential genes are shown in Fig. 1D, including antigen processing and presentation process. These findings indicate that CD14⁺ monocytes with compromised immune potential were unable to activate T lymphocytes.

Monocytes were classified as classical (CD14⁺CD16⁻CCR2⁺CD38⁺), intermediate (CD14⁺CD16⁺CCR2⁺/CCR2⁻CD38⁺), and non-classical (CD14⁻CD16⁺CCR2⁻CD38⁻) (supplementary figure S2). We observed that patients with NDMM had an increased proportion of CCR2⁺ inflammatory intermediate monocytes in the bone marrow compared with HCs ($p = 0.002$, Fig. 1E), and the mean fluorescence intensity (MFI) of the surface co-stimulatory signaling molecules CD86 ($p = 0.0362$), CD80 ($p = 0.0243$), and HLA-DR ($p = 0.0452$) in this subset was decreased (Fig. 1E). The proportion of CCR2⁻ intermediate monocytes was higher in patients with NDMM than in HCs ($p < 0.0001$), with decreased MFI for CD80 ($p = 0.02$) and HLA-DR ($p = 0.0424$; Fig. 1F). There was no difference in the proportion of classical monocytes between NDMM and HCs, and the MFI of the surface molecules CD86 ($p = 0.0316$) and

HLA-DR ($p = 0.0216$) in this subset was lower in patients with NDMM (Fig. 1G).

Clinical indexes such as β 2-microglobulin, serum calcium and creatinine clearance in patients with MM were related to tumor burden and the severity of the disease. Our results indicated that the proportion of CCR2⁻ intermediate monocytes was positively correlated with serum β 2-microglobulin ($r = 0.3286$, $p = 0.0275$, Fig. 1H), and the MFI of HLA-DR in this subset was negatively correlated with serum calcium ($r = -0.3057$, $p = 0.0389$, Fig. 1H). The MFI of CD86 in CCR2⁺ intermediate monocytes was positively correlated with creatinine clearance ($r = 0.4375$, $p = 0.0038$, Fig. 1H), and the MFI of HLA-DR in the subset was negatively correlated with serum calcium ($r = -0.3738$, $p = 0.0095$, Fig. 1H). The MFI of HLA-DR in classical monocytes was also negatively correlated with serum calcium ($r = -0.3756$, $p = 0.0101$, Fig. 1H). These results suggest that intermediate monocytes in NDMM are redundant within the bone marrow environment. The dysfunction of antigen presentation and co-stimulatory signaling molecules observed in CD14⁺ monocytes from patients with NDMM presented them from presenting antigen peptides and providing secondary activated signals to T-lymphocytes. This dysfunction contributes to immune escape and myeloma pathogenesis.

Upregulation of *ULK2* expression in CD14⁺ monocytes from patients with NDMM

We collected bone marrow samples from ten patients with NDMM (A1-A10) and five HCs (C1-C5), and sorted CD14⁺ monocytes (with a purity above 90%; Supplementary Fig. 3A) for RNA sequencing. The Venn plot, volcano plot, heatmap, GO plot, and Kyoto Encyclopedia of Genes and Genomes (KEGG) enrichment bubble plot are shown in Fig. 2A–E. A total of 12,005 co-expressed genes in patients with MM and HCs are shown in the Venn plot. The volcano plot and heatmap showed 477 differentially expressed genes, consisting of 33 upregulated genes and 444 downregulated genes. The top five biological processes according to the GO analysis were extracellular structure organization, extracellular matrix

(See figure on next page.)

Fig. 1 Abnormal numbers and functional defects of CD14⁺ monocytes in the bone marrow of patients with NDMM. **A** Immune cell clusters in bone marrow as shown by UMAP plot. **B** Incoming and outgoing signal strength of CD14⁺ monocytes according to single-cell sequencing data. **C** Signaling change in CD14⁺ monocytes outgoing interaction. **D** Top 10 GO enrichment analysis of differentially expressed genes. **E** Proportion and MFI values for CD86, CD80, and HLA-DR in CD14⁺CD16⁺CCR2⁺CD38⁺ intermediate monocytes ($n = 45$ patients and $n = 20$ healthy controls). **F** Proportion and MFI values for CD86, CD80, and HLA-DR in CD14⁺CD16⁺CCR2⁻CD38⁺ intermediate monocytes ($n = 45$ patients and $n = 20$ healthy controls). **G** Proportion and MFI values for CD86, CD80, and HLA-DR in CD14⁺CD16⁻CCR2⁺CD38⁺ classical monocytes ($n = 45$ patients and $n = 20$ healthy controls). **H** Correlation analysis. The data were analyzed using unpaired t-tests. **** $p < 0.0001$; *** $p < 0.001$; ** $p < 0.01$; * $p < 0.05$. MFI mean fluorescence intensity, NBM healthy donor bone marrow, NDMM newly-diagnosed multiple myeloma, UMAP Uniform Manifold Approximation and Projection

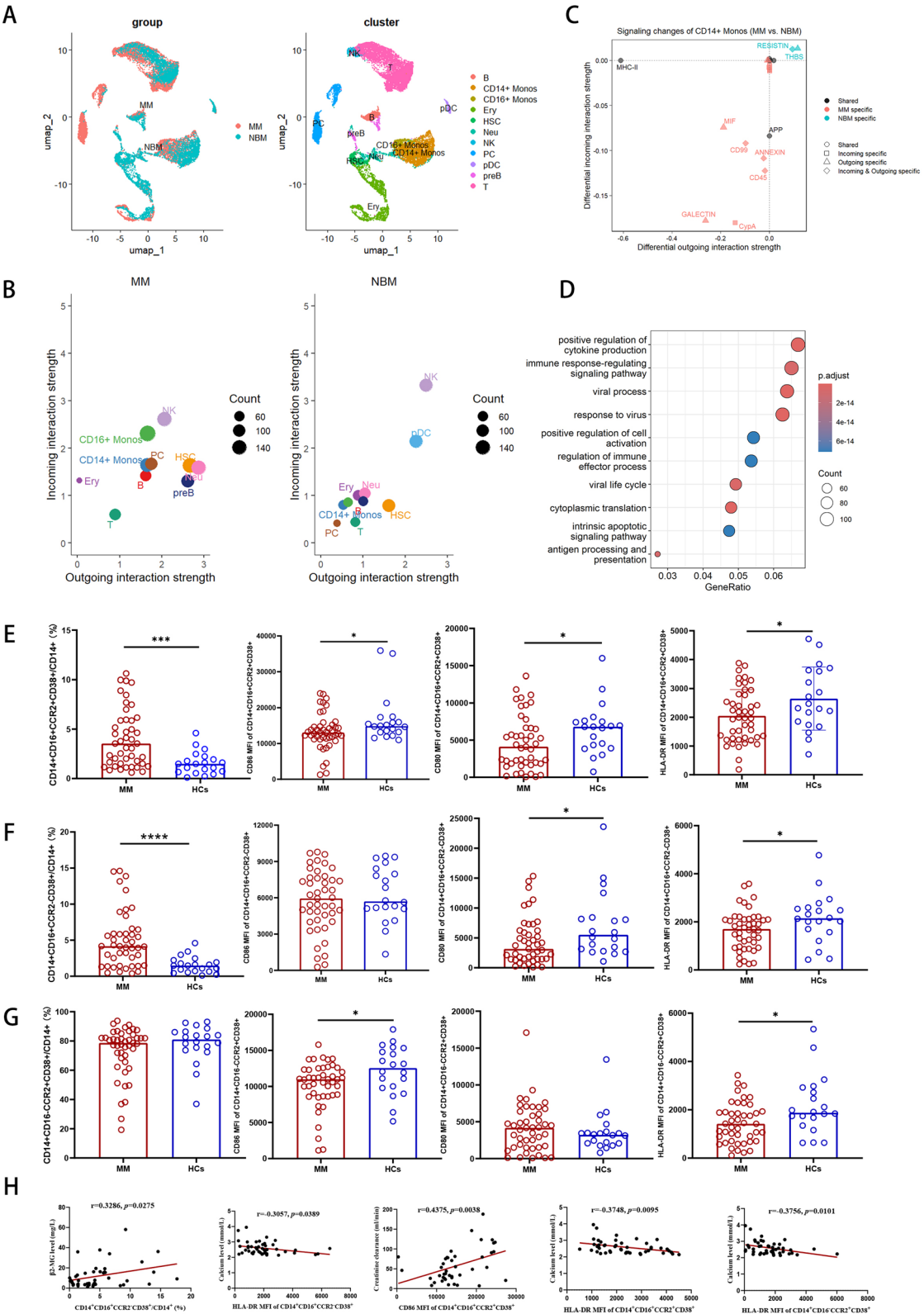


Fig. 1 (See legend on previous page.)

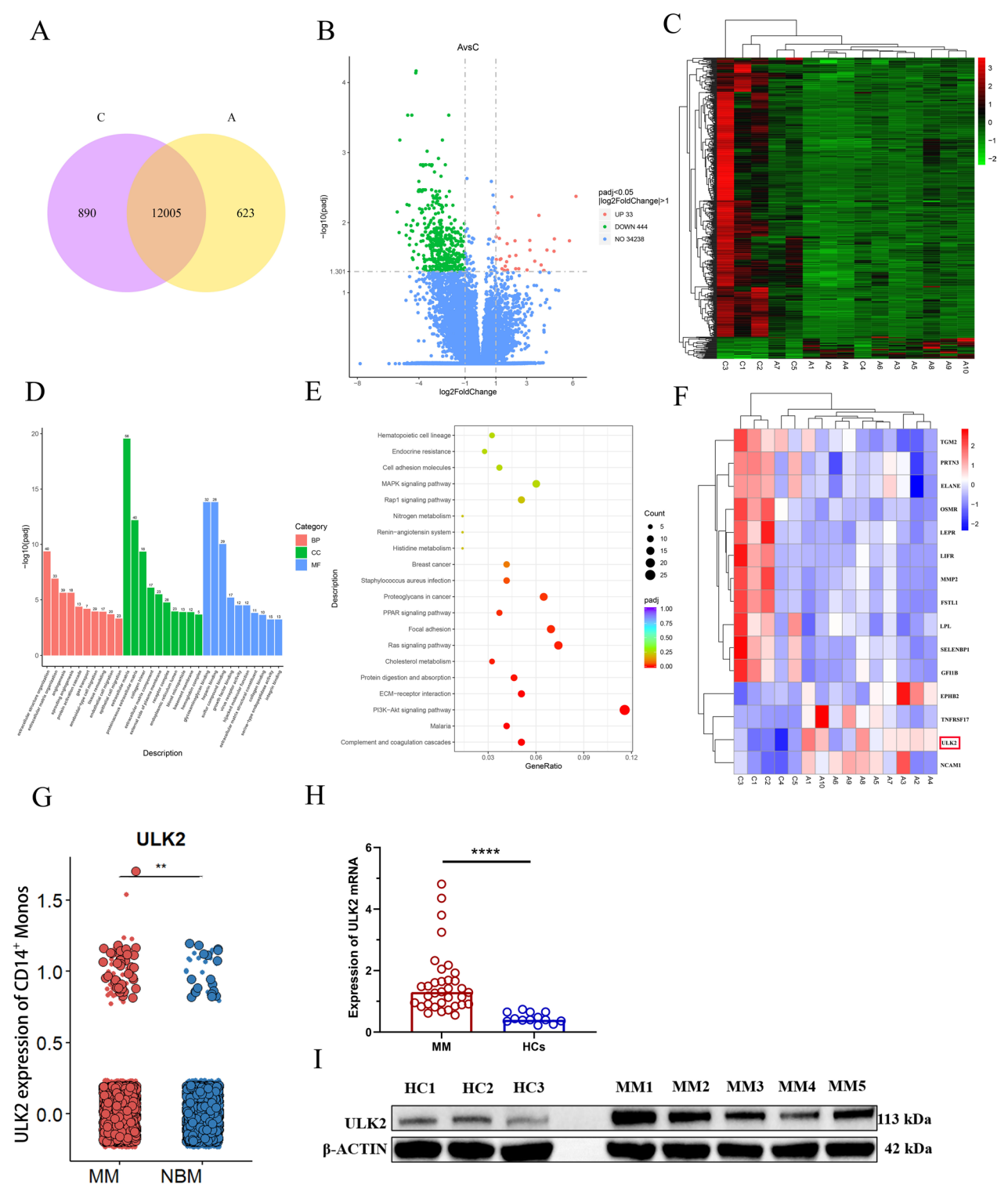


Fig. 2 Upregulated *ULK2* expression in CD14⁺ monocytes from patients with NDMM. **A–E** Venn plot, volcano plot, clustering heatmap, GO plot, and KEGG enrichment bubble plot (n = 10 patients and n = 5 healthy controls). **F** Heatmap of top 15 differentially expressed genes. **G** Expression of *ULK2* in CD14⁺ monocytes of patients with NDMM by analyzing single-cell sequencing data (n = 7 patients and n = 9 healthy controls). **H–I** Expression of *ULK2* mRNA (n = 34 patients and n = 13 healthy controls) and protein (n = 5 patients and n = 3 healthy controls) in CD14⁺ monocytes from patients with NDMM and healthy controls. The data were analyzed using unpaired t-tests. ****p < 0.0001; **p < 0.01. GO Gene Ontology, KEGG Kyoto Encyclopedia of Genes and Genomes, NBM healthy donor bone marrow, NDMM newly-diagnosed multiple myeloma

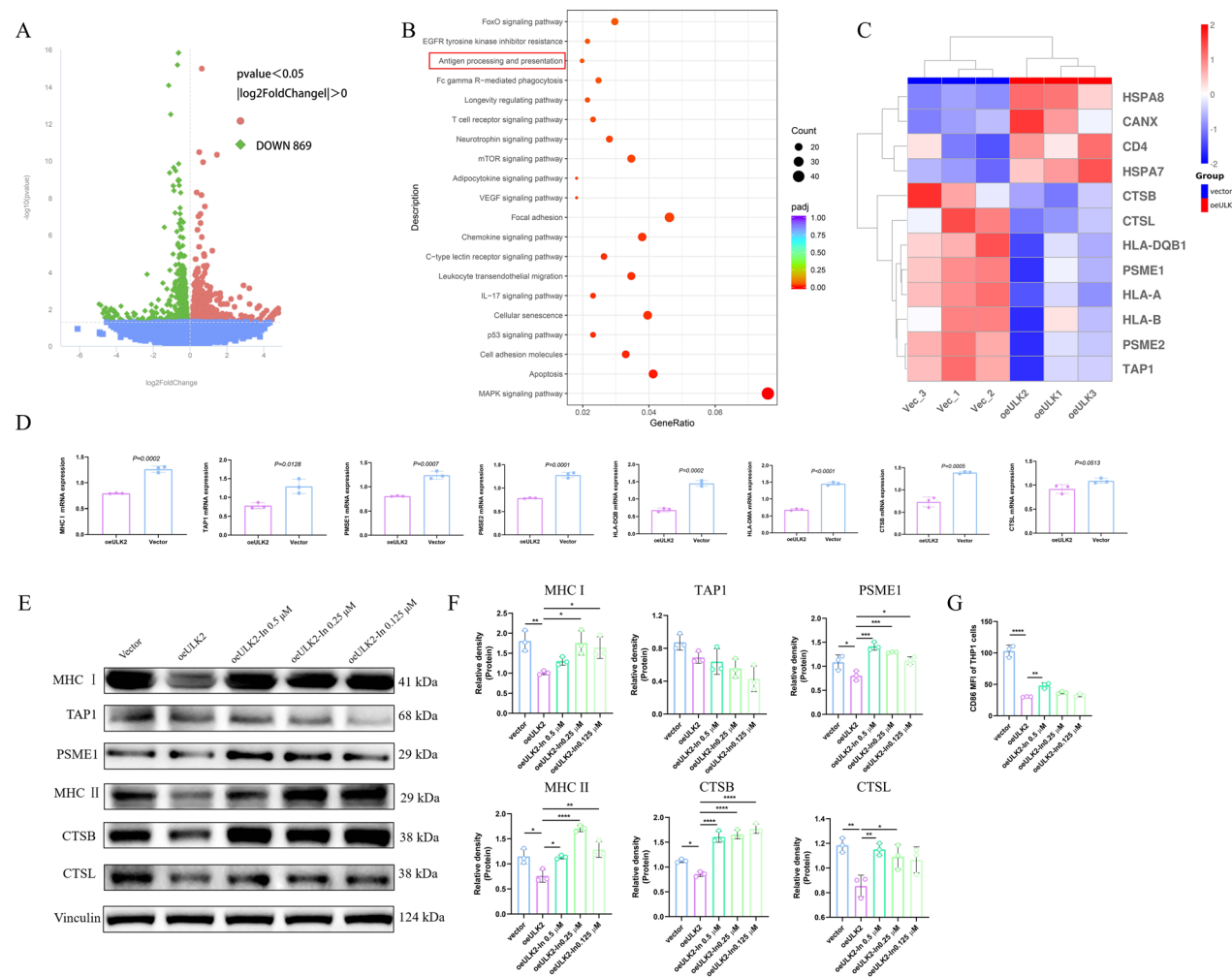


Fig. 3 *ULK2* is involved in the antigen processing and presentation pathway. **A–C** Volcano plot, KEGG enrichment bubble plot, and heatmap of antigen processing and presentation pathway involved in T-lymphocyte activation. **D** mRNA expression of MHC I, TAP1, PSME1/2, HLA-DQB1, HLA-DMA, and CTSL in the THP1 cells overexpressing *ULK2* (oeULK2 THP1). **E–F** Protein expression of MHC I, TAP1, PSME1, MHC II, CTSL, and CTSL in oeULK2 THP1 cells. **G** MFI of CD86 in oeULK2 THP1 cells. The data were analyzed using unpaired t-tests or one-way ANOVA tests (n = 3 biological replicates). *****p* < 0.0001; ***p* < 0.01. KEGG Kyoto Encyclopedia of Genes and Genomes, MFI mean fluorescence intensity

organization, angiogenesis, sprouting angiogenesis, and protein activation cascade. PI3 K-AKT, Ras signaling pathway, local adhesion, and tumor proteoglycan were the top four pathways according to the KEGG enrichment analysis. Notably, the *ULK2* gene, which participated in autophagy, was significantly upregulated in patients with NDMM (Fig. 2F). Moreover, data analysis of GSE124310 revealed that *ULK2* was upregulated in CD14⁺ monocytes from patients with NDMM compared to healthy donors (NBM, *p* < 0.01; Fig. 2G). In our experiment, *ULK2* mRNA expression in CD14⁺ monocytes was significantly higher in 34 patients with NDMM compared to that in 13 HCs (*p* < 0.0001; Fig. 2H). An increase in total *ULK2* expression in CD14⁺ monocytes

from patients with NDMM was verified by WB (Fig. 2I). Therefore, *ULK2* was chosen as our candidate gene to further explore the interaction between CD14⁺ monocytes and T-lymphocytes.

***ULK2* is involved in the antigen processing and presentation pathway in monocytes**

A THP1 cell line overexpressing *ULK2* (oeULK2) was constructed and validated using flow cytometry, PCR, and WB (Supplementary Figures S4 A–C, S5 A). The oeULK2 cells and their control underwent high-throughput RNA sequencing (Datasets were stored in the SRA public repository: <https://www.ncbi.nlm.nih.gov/sra/PRJNA1137432>). The corresponding volcano plot, KEGG

enrichment bubble plot, and heatmap are shown in Fig. 3A–C. The volcano plot showed 575 upregulated differential genes and 869 downregulated differential genes. The top 20 pathways from the KEGG enrichment analysis were listed in Fig. 3B, with the MAPK signaling pathway, apoptosis, focal adhesion, and cellular senescence being the top four pathways. The antigen processing and presentation pathway, involved in T-lymphocyte activation, was validated. Compared with those of control cells, mRNA levels of MHC I, TAP1, PSME1/2, HLA-DQB, HLA-DMA, and CTSB were downregulated in oeULK2 THP1 cells (Fig. 3D). Reduced protein levels of MHC I, PSME1, MHC II, CTSB, and CTSL in oeULK2 THP1 cells were confirmed by WB (Fig. 3E–F). The MFI for CD86 in oeULK2 THP1 cells was decreased (Fig. 3G). The protein levels of MHC I, PSME1, MHC II, CTSB, CTSL, and the MFI of CD86 in oeULK2 THP1 cells were upregulated following exposure to various concentrations of MRT68921 for 48 h (Fig. 3E–G, Supplementary Figure S5B). The MFI of CD86 ($p < 0.0001$) and HLA-DR ($p < 0.0001$) in CD14⁺ monocytes from patients with NDMM was upregulated after exposure to 0.25 μ M MRT68921 for 48 h (Supplementary Figure S5 C–E). These results confirmed that *ULK2* participates in antigen processing and presentation pathways in CD14⁺ monocytes.

Activity of CD3⁺ T-lymphocytes was suppressed by CD14⁺ monocytes in NDMM and alleviated by *ULK2* inhibition

Bone marrow CD14⁺ monocytes and CD3⁺ T-lymphocytes (with a purity above 95%; Supplementary Fig. 3B) from patients with NDMM were collected and sorted. Activated T-lymphocytes were cultured alone, co-cultured with monocytes, and co-cultured with monocytes pretreated with 0.25 μ M MRT68921 for 48 h (Fig. 4A). The activity of CD4⁺/CD8⁺ T-lymphocytes was found to be inhibited after 48 h of co-culture with monocytes, indicated by a decrease in the MFI of CD69, CD25, GZMB, and TNF α (Fig. 4B–C). This was alleviated by co-culturing with CD14⁺ monocytes pretreated with MRT68921. This demonstrated that the *ULK2* gene is involved in the defective antigen presentation and downregulation of surface co-stimulatory molecules observed in CD14⁺ monocytes derived from patients with MM.

High expression of *ULK2* in CD14⁺ monocytes promoted tumor growth and suppressed T-lymphocytes in the MM xenograft model

RPML-8226 MM cells were subcutaneously implanted in mice, and human CD3⁺ T-lymphocytes and *ULK2*^{high} or *ULK2*^{low/-} CD14⁺ monocytes were infused to reconstitute immunity (Fig. 5A). Tumor growth was significantly accelerated by the infusion of *ULK2*^{high} monocytes (Fig. 5B–D). PET/CT images confirmed tumor growth

(Fig. 5E). The MFI values for CD69 ($p < 0.05$), GZMB ($p < 0.01$), and TNF α ($p < 0.01$) of CD3⁺ T-lymphocytes from the tumor tissue were notably downregulated after infusion of *ULK2*^{high} monocytes compared to infusion with *ULK2*^{low/-} monocytes (Fig. 5F–H, Supplementary Figure S6 A). The serum IFN γ level was lower in the *ULK2*^{high} monocytes group ($p < 0.05$, Fig. 5I).

Discussion

MM is incurable and highly prone to relapse. Immunosuppressive cells in the tumor microenvironment inhibit endogenous T-lymphocyte activity. The abnormal number of CD14⁺ monocytes in patients with MM is correlated with inferior outcomes [11, 16]. We found that bone marrow CD14⁺ monocytes from patients with NDMM inhibited T-lymphocyte activation, as they showed abnormal numbers, defective antigen presentation, and downregulated surface co-stimulatory molecules. *ULK2* was upregulated in this subset. Inhibition of *ULK2* in CD14⁺ monocytes alleviated the suppression of T-lymphocytes. This study elucidates the mechanisms regulating T-lymphocytes and the bone marrow environment by examining the interaction between CD14⁺ monocytes and T-lymphocytes, as well as the downstream signaling mechanism through in vitro and in vivo experiments.

Monocytes are crucial to the development of MM and the formation of a suppressive immune microenvironment. In our study, we found an increased proportion of bone marrow intermediate monocytes in MM samples, consistent with the results reported by Damasceno [17]. Bolzoni et al. [18] indicated that higher levels of bone marrow CD14⁺CD16⁺ intermediate monocytes in MM enhance osteoclastogenesis. In COVID-19, increased numbers of CCR2⁺ monocytes are considered the main source of pro-inflammatory cytokines (such as IL6, TNF, IL1 β , and IL8), contributing to the so-called ‘inflammatory storm’ [19]. CCR2⁺ inflammatory monocytes have been shown to activate NK cells and memory CD8⁺ T lymphocytes, which are involved in the antimicrobial response [20]. Pro-inflammatory cytokines such as IL1 β , IL6, and TNF α are verified to be increased in MM, promoting tumor growth and disease progression [21, 22]. The redundant inflammatory monocytes in MM may be responsible for the excessive levels of inflammatory cytokines in the bone marrow environment, facilitating the proliferation and survival of malignant plasma cells. We hypothesized that defective antigen presentation and downregulation of surface co-stimulatory molecules observed in bone marrow CD14⁺ monocytes from patients with MM were responsible for their inability to sufficiently activate immune cells, resulting in immune escape. Zavidij et al. [2] found that the bone marrow of patients with MM was enriched with a population of

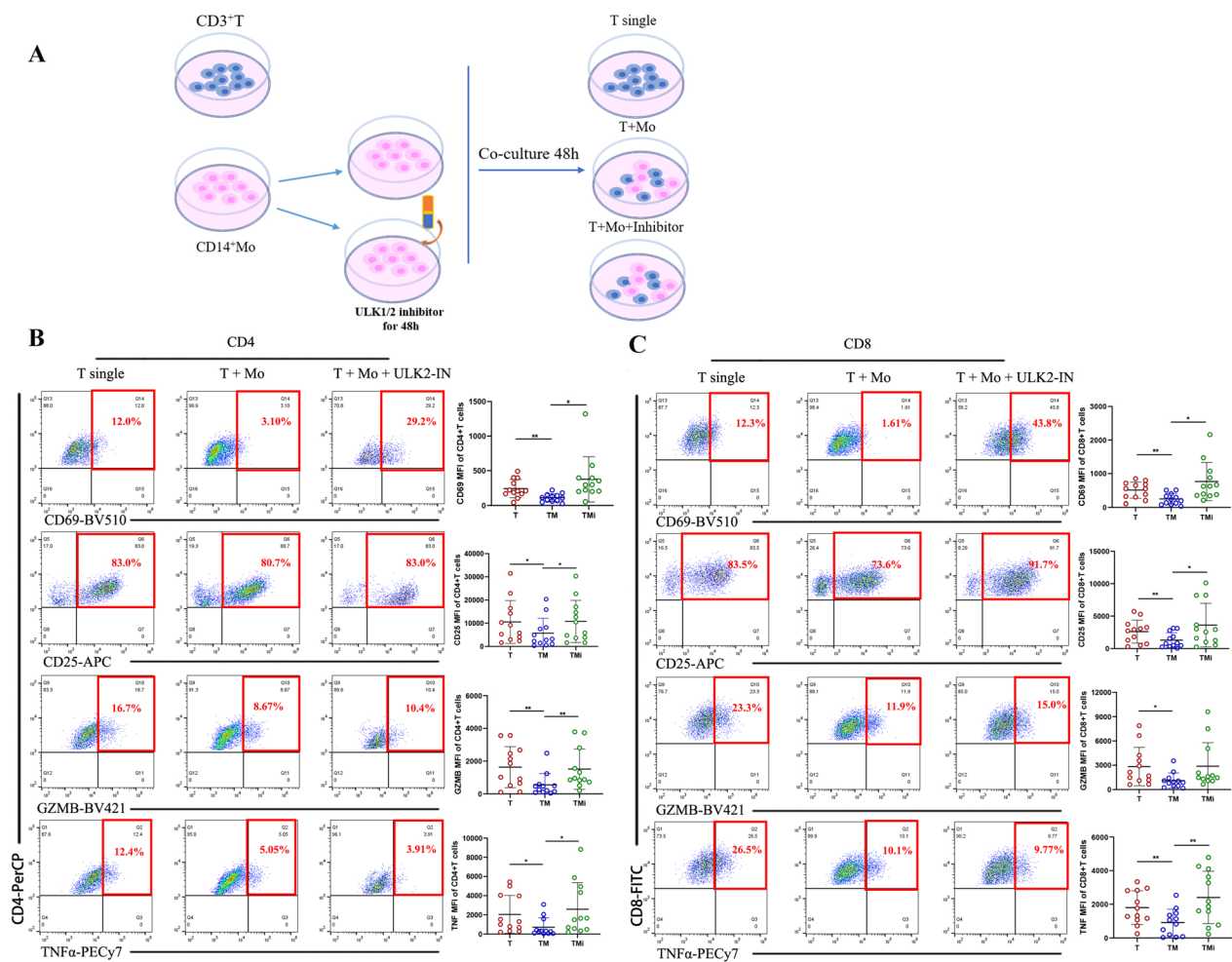


Fig. 4 Activation of CD3⁺ T-lymphocytes was inhibited by CD14⁺ monocytes in co-culture assays, and *ULK2* inhibition prevented this outcome. **A** Schedule for the co-culture assays. **B** Gating strategy to detect the activation of CD4⁺ T-lymphocytes from the co-culture assays and MFI values for CD69, CD25, GZMB and TNFα in CD4⁺ T-lymphocytes. **C** Gating strategy to detect the activation of CD8⁺ T-lymphocytes from the co-culture assay and MFI values for CD69, CD25, GZMB and TNFα in CD8⁺ T-lymphocytes. The data were analyzed using one-way ANOVA tests (n = 12 patients). ***p* < 0.01; **p* < 0.05. MFI, mean fluorescence intensity

CD14⁺ monocytes showing high expression of the interferon type I gene and had an impaired antigen-presenting capacity, which in turn promotes the proliferation of MM cells and inhibits T-lymphocyte activation. Single-cell sequencing of dendritic cells (DCs) and monocytes from patients with MM revealed that monocyte-derived DCs developed from intermediate monocytes. Conventional DC2, monocyte-derived DCs and intermediate monocytes have been characterized by impaired antigen processing and presenting capacity, and by reduced interferon-regulatory factor (IRF1)-regulated activity [23]. The proliferation of T lymphocytes was significantly inhibited when mouse DC2.4 cells and RAW264.7 cells with IRF1 knockdown were co-cultured with CD4⁺ T cells.

ULK2, along with its homolog *ULK1*, belongs to the serine/threonine kinase family. Their protein kinase domains have an identity of 78% [15], and their biological functions had been assumed to be redundant. *ULK1* and *ULK2* are crucial components of the protein complex participating in the regulation and signaling of autophagy [24], and can either suppress or promote tumor growth in different conditions. *ULK1* has a cytoprotective function in neurons and is an essential component of the autophagy signaling pathway activated under starvation in fibroblasts [15]. Cardiac-specific *ULK1* knockout mice, but not *ULK2* knockout mice, are inherently prone to a rapidly developing type of cardiomyopathy, heart failure, and early death [25]. *ULK1*, but not *ULK2*, also improves

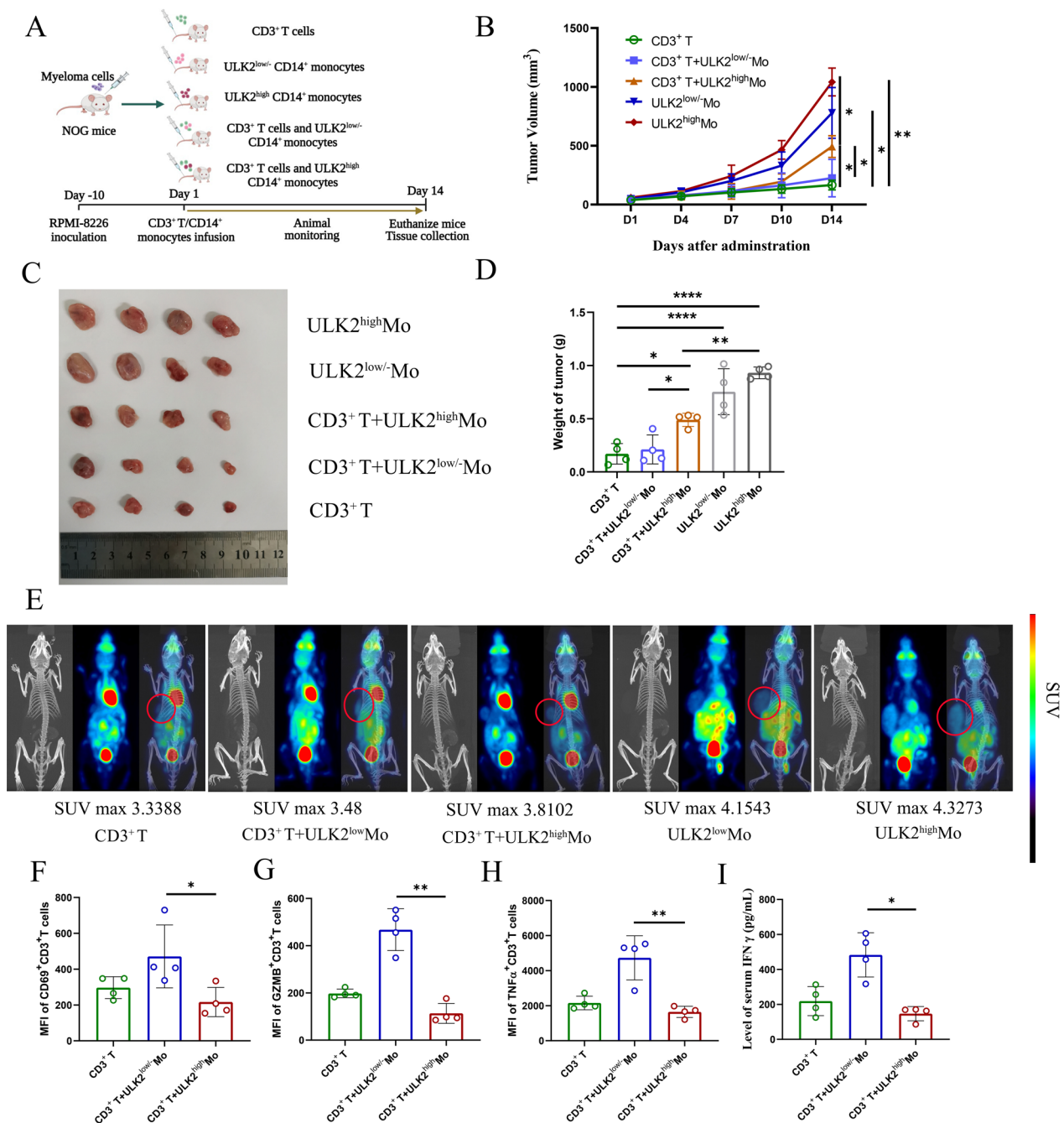


Fig. 5 *ULK2^{high}* CD14⁺ monocytes promoted tumor growth and suppressed T-lymphocytes in a MM mice model. **A** Schedule for the RPMI-8226 xenograft model experiment (n = 4 mice/group). The diagram was drawn using BioRender.com. **B** Tumor volume for the five experimental groups. **C** Mice tumor tissues were dissected at the end of the experiment. **D** Tumor weight for the five experimental groups. **E** Representative PET/CT images for the five experimental groups. **F–H** MFI values for CD69, GZMB, and TNFα in CD3⁺ T-lymphocytes from tumor tissues collected from three treatment groups. **I** Serum interferon γ levels for each group. The data were analyzed using one-way ANOVA tests or two-way ANOVA tests. *****p* < 0.0001; ***p* < 0.01; **p* < 0.05. MM multiple myeloma, MFI mean fluorescence intensity, PET/CT positron emission tomography/computed tomography

the insulin response induced by exercise training in skeletal muscle [26].

Notably, some studies have proposed that *ULK2* has functions that are different from those of *ULK1*. *ULK2*

is involved in the determination of cell fate, metabolism, transcriptional control, and tumorigenesis [15, 27]. Ro et al. [28] suggested that *ULK2* and *ULK1* play different roles in lipid metabolism in adipocytes, with

downregulation of *ULK2* increasing fatty acid oxidation, and downregulation of *ULK1* inhibiting it instead. *ULK1* and *ULK2* also play contrasting roles in insulin-stimulated blood glucose uptake. *ULK2* deficiency in skeletal muscle contributes to the accumulation of insoluble ubiquitinated protein, resulting in the impairment of muscle force, and the degeneration and atrophy of myofibers [29]. Silencing of *ULK2* by methylation promotes cell migration and epithelial-mesenchymal transition through autophagy induction in gastric cancers [30]. PKC $\alpha/1$ deficiency in colorectal cancer activates *ULK2* in intestinal epithelial cells; the accumulated activated *ULK2* phosphorylates TBK1, promotes TBK1-STING-IRF3-mediated IFN signaling, increases infiltration of CD8⁺ T lymphocytes and triggers anti-tumor responses [31]. In acute myelocytic leukemia, *ULK2* plays a considerable role in the enhancement of autophagy-mediated chemoresistance in SORE6⁺ cells, promoting cancer development and recurrence [32]. In our study (Fig. 6), we found that the expression of *ULK2* was upregulated in CD14⁺ monocytes from patients with NDMM. We verified that high expression of the *ULK2* gene in THP1 cells

was accompanied by a deficient antigen processing and presentation capacity, and by decreased expression of MHC I, TAP1, PSME1, MHC II, CTSB, CTSL, and CD86. Co-culture experiments revealed that bone marrow CD14⁺ monocytes from patients with NDMM samples suppressed T-lymphocyte activity, and that treatment of CD14⁺ monocytes with a *ULK1/ULK2* inhibitor alleviated T-lymphocyte suppression. In vivo experiments found that *ULK2*^{high} CD14⁺ monocytes suppressed the activity of T-lymphocytes and promoted tumor growth in mice models for MM. The MHC I and MHC II complexes are widely acknowledged to present antigens to T-lymphocytes [33]. The cytotoxicity, cytokine production, and activation of other immune cells by T-lymphocytes were significantly impaired owing to the deficiency of essential MHC molecules in *ULK2*^{high} CD14⁺ monocytes. Coincidentally, Yamamoto et al. [34] demonstrated that MHC I molecules are selectively targeted for lysosomal degradation through an autophagy-dependent mechanism involving the autophagy cargo receptor NBR1 in pancreatic ductal adenocarcinoma cells. Additionally, the inhibition of autophagy improved antigen presentation

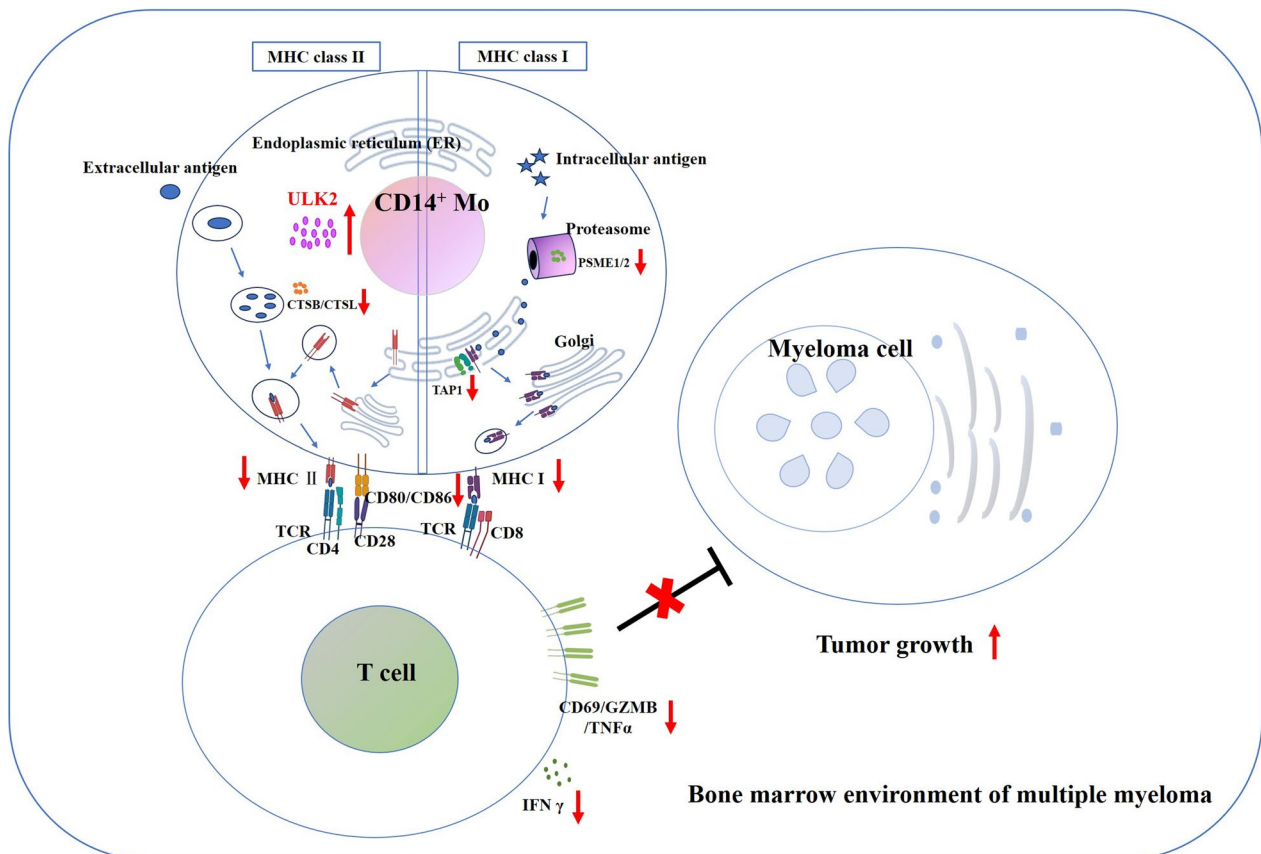


Fig. 6 Schematic overview of how CD14⁺ monocytes high-expressing *ULK2* suppress T-lymphocyte activation and promote tumor growth in multiple myeloma

by restoring surface MHC I level. This is a feature of *ULK2* that differs from previous discoveries. Therefore, we hypothesize that *ULK2^{high}* CD14⁺ monocytes play a key role in the formation of a suppressive bone marrow environment and the pathological mechanism of immune escape that characterizes MM.

MRT68921 specifically inhibits ULK1/ULK2 protein kinase activity [35], and it is unknown whether it affects T-lymphocyte function through the inhibition of *ULK1* in the co-culture assay. The mechanism by which *ULK2* present in CD14⁺ monocytes affects the antigen processing and presentation pathway needs further exploration. Several studies have indicated that the expression and activity of MHC I and MHC II were regulated by interferon signal, mTOR, Wnt, MAPK, Hippo signaling, and JAK/STAT signaling pathway [36–38]. It is also crucial to confirm that *ULK2* can regulate the activity of T-lymphocytes in the monocyte-specific conditional knockout murine model.

Conclusion

We demonstrated that CD14⁺ monocytes from patients with NDMM disrupt the antigen processing and presentation pathway. This disruption affects T-lymphocyte activity and attenuates their ability to kill malignant cells and secrete cytokines. This study lays the foundation for understanding the immuno-suppressive environment, improving the efficacy of immunotherapy based on T-lymphocytes, and developing new therapeutic targets.

Abbreviations

MM	Multiple myeloma
NDMM	Newly-diagnosed multiple myeloma
ULK2	Unc-51 like autophagy activating kinase 2
BCMA	B-cell maturation antigen
CART	Chimeric Antigen Receptor T-cell Immunotherapy
HCS	Healthy controls
GO	Gene Ontology
WB	Western blots
RT-qPCR	Real-time quantitative PCR
GZMB	Granzyme B
IFN γ	Interferon γ
MFI	Mean fluorescence intensity
KEGG	Kyoto Encyclopedia of Genes and Genomes
DCs	Dendritic cells
PET/CT	Positron emission tomography / computed tomography

Supplementary Information

The online version contains supplementary material available at <https://doi.org/10.1186/s12967-025-06516-0>.

Additional file 1

Acknowledgements

Not applicable.

Author contributions

RF and ZL designed the project and proofread the manuscript. FP conducted the experiments, analysed the data and finished the manuscript. FJ, NL, HW, NM, HL, and KD participated in the experimental work and collected clinical data. All authors checked and approved the final manuscript.

Funding

This work was supported by National Natural Science Foundation Project (Grant no.82400242), Tianjin Municipal Natural Science Foundation (Grant no. 23 JQJNC00870), Tianjin Education Commission Research Project (Grant no. 2023 KJ112), Tianjin Health Research Project (Grant No. TJWJ2024QN008), Tianjin Science and Technology Planning Project (Grant no. 24ZXZSY00090), China postdoctoral science foundation (Grant no. 2023MT42624).

Availability of data and materials

High-throughput RNA sequencing datasets can be found in the Sequence Read Archive public repository: <https://www.ncbi.nlm.nih.gov/sra/PRJNA1138781>, <https://www.ncbi.nlm.nih.gov/sra/PRJNA1137432>.

Declarations

Ethics approval and consent to participate

Ethics Committee and Experimental Animal Welfare Ethics Committee of Tianjin Medical University General Hospital permitted this project (IRB2023-KY-325, IRB2023-DWFL-397). All participants signed written informed consent.

Consent for publication

Not applicable.

Competing interests

All authors declare no competing of interest.

Author details

¹Department of Hematology, Tianjin Medical University General Hospital, 154 Anshan Street, Heping District, Tianjin 300052, People's Republic of China.

²Tianjin Key Laboratory of Bone Marrow Failure and Malignant Hemopoietic Clone Control, Tianjin 300052, People's Republic of China. ³Tianjin Institute of Hematology, Tianjin 300052, People's Republic of China.

Received: 18 March 2025 Accepted: 18 April 2025

Published online: 07 May 2025

References

- Robak P, Drozd I, Szemraj J, Robak T. Drug resistance in multiple myeloma. *Cancer Treat Rev*. 2018;70:199–208.
- Zavidij O, Haradhvala NJ, Mouhieddine TH, Sklavenitis-Pistofidis R, Cai S, Reidy M, et al. Single-cell RNA sequencing reveals compromised immune microenvironment in precursor stages of multiple myeloma. *Nat Cancer*. 2020;1(5):493–506.
- Rodríguez-Otero P, Paiva B, Engelhardt M, Prósper F, San Miguel JF. Is immunotherapy here to stay in multiple myeloma? *Haematologica*. 2017;102(3):423–32.
- Maura F, Boyle EM, Coffey D, MacLachlan K, Gaggar D, Diamond B, et al. Genomic and immune signatures predict clinical outcome in newly diagnosed multiple myeloma treated with immunotherapy regimens. *Nat Cancer*. 2023;4(12):1660–74.
- Botta C, Perez C, Larrayoz M, Puig N, Cedena MT, Termini R, et al. Large T cell clones expressing immune checkpoints increase during multiple myeloma evolution and predict treatment resistance. *Nat Commun*. 2023;20(14):5825.
- Friedrich MJ, Neri P, Kehl N, Michel J, Steiger S, Kilian M, et al. The pre-existing T cell landscape determines the response to bispecific T cell engagers in multiple myeloma patients. *Cancer Cell*. 2023;41(4):711–725.e6.
- Dhodapkar KM, Cohen AD, Kaushal A, Garfall AL, Manalo RJ, Carr AR, et al. Changes in bone marrow tumor and immune cells correlate with

- durability of remissions following BCMA CAR T therapy in Myeloma. *Blood Cancer Discov.* 2022;3(6):490–501.
8. Swamydas M, Murphy EV, Ignatz-Hoover JJ, Malek E, Driscoll JJ. Deciphering mechanisms of immune escape to inform immunotherapeutic strategies in multiple myeloma. *J Hematol Oncol.* 2022;15(1):17.
 9. Gabrilovich DI, Ostrand-Rosenberg S, Bronte V. Coordinated regulation of myeloid cells by tumours. *Nat Rev Immunol.* 2012;12(4):253–68.
 10. Ugel S, Canè S, De Sanctis F, Bronte V. Monocytes in the Tumor Microenvironment. *Annu Rev Pathol.* 2021;24(16):93–122.
 11. Sklaventis-Pistofidis R, Aranha MP, Redd RA, Baginska J, Haradhvala NJ, Hallisey M, et al. Immune biomarkers of response to immunotherapy in patients with high-risk smoldering myeloma. *Cancer Cell.* 2022;40(11):1358–1373.e8.
 12. Tirier SM, Mallm JP, Steiger S, Poos AM, Awwad MHS, Giesen N, et al. Subclone-specific microenvironmental impact and drug response in refractory multiple myeloma revealed by single-cell transcriptomics. *Nat Commun.* 2021;12(1):6960.
 13. Li W, Zhang B, Cao W, Zhang W, Li T, Liu L, et al. Identification of potential resistance mechanisms and therapeutic targets for the relapse of BCMA CAR-T therapy in relapsed/refractory multiple myeloma through single-cell sequencing. *Exp Hematol Oncol.* 2023;12(1):44.
 14. Sprangers S, de Vries TJ, Everts V. Monocyte heterogeneity: consequences for monocyte-derived immune cells. *J Immunol Res.* 2016;2016:1475435.
 15. Lee EJ, Tournier C. The requirement of uncoordinated 51-like kinase 1 (ULK1) and ULK2 in the regulation of autophagy. *Autophagy.* 2011;7(7):689–95.
 16. Edwards CV, Hassan H, Yildirim C, Ferri G, Verma KP, Murray Horwitz ME, et al. Peripheral blood monocyte count is a dynamic prognostic biomarker in multiple myeloma. *Blood Adv.* 2023;7(4):482–90.
 17. Damasceno D, Almeida J, Teodosio C, Sanoja-Flores L, Mayado A, Pérez-Pons A, et al. Monocyte subsets and serum inflammatory and bone-associated markers in monoclonal gammopathy of undetermined significance and multiple myeloma. *Cancers (Basel).* 2021;13(6):1454.
 18. Bolzoni M, Ronchetti D, Storti P, Donofrio G, Marchica V, Costa F, et al. IL21R expressing CD14+CD16+ monocytes expand in multiple myeloma patients leading to increased osteoclasts. *Haematologica.* 2017;102(4):773–84.
 19. Gibellini L, De Biasi S, Paolini A, Borella R, Boraldi F, Mattioli M, et al. Altered bioenergetics and mitochondrial dysfunction of monocytes in patients with COVID-19 pneumonia. *EMBO Mol Med.* 2020;12(12):e13001.
 20. Soudja SM, Ruiz AL, Marie JC, Lauvau G. Inflammatory monocytes activate memory CD8(+) T and innate NK lymphocytes independent of cognate antigen during microbial pathogen invasion. *Immunity.* 2012;37(3):549–62.
 21. Robak P, Węglowska E, Drózd I, Mikulski D, Jarych D, Ferlińska M, et al. Cytokine and chemokine profile in patients with multiple myeloma treated with bortezomib. *Mediators Inflamm.* 2020;6(2020):1835836.
 22. Gu J, Huang X, Zhang Y, Bao C, Zhou Z, Jin J. Cytokine profiles in patients with newly diagnosed multiple myeloma: survival is associated with IL-6 and IL-17A levels. *Cytokine.* 2021;138: 155358.
 23. Jiang J, Xiang J, Chen M, Wan Y, Zhong L, Han X, et al. Distinct mechanisms of dysfunctional antigen-presenting DCs and monocytes by single-cell sequencing in multiple myeloma. *Cancer Sci.* 2023;114(7):2750–60.
 24. Kim J, Kundu M, Viollet B, Guan KL. AMPK and mTOR regulate autophagy through direct phosphorylation of Ulk1. *Nat Cell Biol.* 2011;13(2):132–41.
 25. Harris MP, Zhang QJ, Cochran CT, Ponce J, Alexander S, Kronemberger A, et al. Perinatal versus adult loss of ULK1 and ULK2 distinctly influences cardiac autophagy and function. *Autophagy.* 2022;18(9):2161–77.
 26. Drake JC, Wilson RJ, Cui D, Guan Y, Kundu M, Zhang M, et al. Ulk1, Not Ulk 2, Is required for exercise training-induced improvement of insulin response in skeletal muscle. *Front Physiol.* 2021;12: 732308.
 27. Shin SH, Lee EJ, Chun J, Hyun S, Kang SS. ULK2 Ser 1027 phosphorylation by PKA regulates its nuclear localization occurring through karyopherin beta 2 recognition of a PY-NLS Motif. *PLoS ONE.* 2015;10(6): e0127784.
 28. Ro SH, Jung CH, Hahn WS, Xu X, Kim YM, Yun YS, et al. Distinct functions of Ulk1 and Ulk2 in the regulation of lipid metabolism in adipocytes. *Autophagy.* 2013;9(12):2103–14.
 29. Fuqua JD, Mere CP, Kronemberger A, Blomme J, Bae D, Turner KD, et al. ULK2 is essential for degradation of ubiquitinated protein aggregates and homeostasis in skeletal muscle. *FASEB J.* 2019;33(11):11735–45.
 30. Motoo I, Nanjo S, Ando T, Yamashita S, Ushijima T, Yasuda I. Methylation silencing of ULK2 via epithelial-mesenchymal transition causes transformation to poorly differentiated gastric cancers. *Gastric Cancer.* 2022;25(2):325–35.
 31. Linares JF, Zhang X, Martinez-Ordoñez A, Duran A, Kinoshita H, Kasashima H, et al. PKC α inhibition activates an ULK2-mediated interferon response to repress tumorigenesis. *Mol Cell.* 2021;81(21):4509–4526.e10.
 32. Lai J, Yang C, Shang C, Chen W, Chu MP, Brandwein J, et al. ULK2 is a key pro-autophagy protein that contributes to the high chemoresistance and disease relapse in FLT3-mutated acute Myeloid Leukemia. *Int J Mol Sci.* 2024;25(1):646.
 33. Pishesha N, Harmand TJ, Ploegh HL. A guide to antigen processing and presentation. *Nat Rev Immunol.* 2022;22(12):751–64.
 34. Yamamoto K, Venida A, Yano J, Biancur DE, Kakiuchi M, Gupta S, Sohn AS, Mukhopadhyay S, Lin EY, Parker SJ, Banh RS, et al. Autophagy promotes immune evasion of pancreatic cancer by degrading MHC-I. *Nature.* 2020;581:7806.
 35. Petherick KJ, Conway OJL, Mpamhanga C, Osborne SA, Kamal A, Saxty B, et al. Pharmacological Inhibition of ULK1 kinase blocks mammalian target of rapamycin (mTOR)-dependent autophagy. *J Biol Chem.* 2015;290(18):11376–83.
 36. Axelrod ML, Cook RS, Johnson DB, Balko JM. Biological consequences of MHC-II expression by tumor cells in cancer. *Clin Cancer Res.* 2019;25(8):2392–402.
 37. Zeng Z, Gu SS, Ouadaoui N, Tymm C, Yang L, Wong CJ, et al. Hippo signaling pathway regulates cancer cell-intrinsic MHC-II expression. *Cancer Immunol Res.* 2022;10(12):1559–69.
 38. Sari G, Rock KL. Tumor immune evasion through loss of MHC class-I antigen presentation. *Curr Opin Immunol.* 2023;83: 102329.

Publisher's Note

Springer Nature remains neutral with regard to jurisdictional claims in published maps and institutional affiliations.